

# Temporally and spatially resolved photoluminescence investigation of (11 $\bar{2}$ 2) semi-polar InGaN/GaN multiple quantum wells grown on nanorod templates

B. Liu, R. Smith, M. Athanasiou, X. Yu, J. Bai, and T. Wang

Citation: *Appl. Phys. Lett.* **105**, 261103 (2014); doi: 10.1063/1.4905191

View online: <http://dx.doi.org/10.1063/1.4905191>

View Table of Contents: <http://aip.scitation.org/toc/apl/105/26>

Published by the [American Institute of Physics](#)

---

## Articles you may be interested in

[Great emission enhancement and excitonic recombination dynamics of InGaN/GaN nanorod structures](#)  
*Applied Physics Letters* **103**, 101108 (2013); 10.1063/1.4820794

[Stokes shift in semi-polar \(11 \$\bar{2}\$ 2\) InGaN/GaN multiple quantum wells](#)  
*Applied Physics Letters* **108**, 031108 (2016); 10.1063/1.4940396

[Radiative recombination mechanisms in polar and non-polar InGaN/GaN quantum well LED structures](#)  
*Applied Physics Letters* **109**, 151110 (2016); 10.1063/1.4964842

[Microstructure investigation of semi-polar \(11-22\) GaN overgrown on differently designed micro-rod array templates](#)  
*Applied Physics Letters* **109**, 241906 (2016); 10.1063/1.4972403

[Characterization of InGaN-based nanorod light emitting diodes with different indium compositions](#)  
*Journal of Applied Physics* **111**, 113103 (2012); 10.1063/1.4725417

[Droop in InGaN light-emitting diodes: A differential carrier lifetime analysis](#)  
*Applied Physics Letters* **96**, 103504 (2010); 10.1063/1.3330870

---



**THE WORLD'S RESOURCE FOR  
VARIABLE TEMPERATURE  
SOLID STATE CHARACTERIZATION**



OPTICAL STUDIES SYSTEMS



SEEBECK STUDIES SYSTEMS



MICROPROBE STATIONS



HALL EFFECT STUDY SYSTEMS AND MAGNETS

[WWW.MMR-TECH.COM](http://WWW.MMR-TECH.COM)

# Temporally and spatially resolved photoluminescence investigation of (11 $\bar{2}2$ ) semi-polar InGaN/GaN multiple quantum wells grown on nanorod templates

B. Liu, R. Smith, M. Athanasiou, X. Yu, J. Bai, and T. Wang<sup>a)</sup>

Department of Electronic and Electrical Engineering, University of Sheffield, Mappin Street, Sheffield S1 3JD, United Kingdom

(Received 6 April 2014; accepted 16 December 2014; published online 29 December 2014)

By means of time-resolved photoluminescence (PL) and confocal PL measurements, temporally and spatially resolved optical properties have been investigated on a number of In<sub>x</sub>Ga<sub>1-x</sub>N/GaN multiple-quantum-well (MQW) structures with a wide range of indium content alloys from 13% to 35% on (11 $\bar{2}2$ ) semi-polar GaN with high crystal quality, obtained through overgrowth on nanorod templates. With increasing indium content, the radiative recombination lifetime initially increases as expected, but decreases if the indium content further increases to 35%, corresponding to emission in the green spectral region. The reduced radiative recombination lifetime leads to enhanced optical performance for the high indium content MQWs as a result of strong exciton localization, which is different from the behaviour of c-plane InGaN/GaN MQWs, where quantum confined Stark effect plays a dominating role in emission process. © 2014 AIP Publishing LLC.  
[\[http://dx.doi.org/10.1063/1.4905191\]](http://dx.doi.org/10.1063/1.4905191)

The major achievements in III-nitride optoelectronics have so far been made predominantly on (0001) sapphire. This polar orientation results in internal electric fields due to polarization effects, generating the so-called quantum-confined Stark effect (QCSE). This becomes particularly pronounced in InGaN/GaN material system as a result of the large lattice-mismatch between InGaN and GaN. Consequently, current InGaN-based emitters suffer from a reduced overlap between the electron and hole wave functions, thus leading to a reduction in optical efficiency. It becomes even worse when the emission shifts towards longer wavelengths, such as the green spectral region, since higher indium composition alloys are required and thus the QCSE becomes even stronger as a result of the increased lattice mismatch. This is the major mechanism responsible for the well-known “green-gap” issue. One of the promising approaches is to grow InGaN/GaN multiple quantum well (MQW) structures along non-polar or semi-polar orientations, which can eliminate or significantly reduce the polarization induced electric fields, the major cause of QCSE.<sup>1-5</sup> Therefore, the growth of InGaN-based emitters along a non-polar or semi-polar direction is particularly important for long wavelength applications, where a high indium content is required. However, so far there has been no systematic study on the optical properties of InGaN/GaN MQWs with a high indium content grown on sapphire along non-polar and semi-polar directions. Part of the reason is most likely due to the significantly lower crystal quality achieved in such growth on sapphire. Very recently, we have developed a cost-effective overgrowth approach based on nanorod templates fabricated using self-organized nickel nanomasks, leading to an improved crystal quality in both (11 $\bar{2}0$ ) non-polar and (11 $\bar{2}2$ ) semi-polar GaN on sapphire.<sup>6,7</sup>

Theoretically, it would be the most convenient to study the optical properties using non-polar InGaN/GaN MQWs with high indium content, as it can simplify the analysis as a result of the elimination of QCSE. However, compared with c-plane and non-polar orientations, such as (11 $\bar{2}0$ ) GaN grown on *R-plane* sapphire, there is another major advantage for InGaN/GaN MQWs grown along the (11 $\bar{2}2$ ) semi-polar direction, i.e., an enhanced indium incorporation can be achieved as a result of a significantly lower indium chemical potential.<sup>8</sup> This is also crucial in achieving high indium content InGaN/GaN MQWs with improved performance, as it means that higher indium content can be potentially obtained even at high growth temperatures.

In this letter, by means of time resolved photoluminescence (TRPL) and confocal PL measurements, we have carried out temporally and spatially resolved PL investigations on In<sub>x</sub>Ga<sub>1-x</sub>N/GaN MQWs with a wide range of indium content (13% ≤ *x* ≤ 35%) on (11 $\bar{2}2$ ) semi-polar GaN with significantly improved crystal quality grown on nanorod templates. Such a systematic study on (11 $\bar{2}2$ ) semipolar InGaN/GaN MQW with high indium content has not yet been reported, even on very expensive free-standing semi-polar GaN substrates.<sup>9-14,21</sup>

The (11 $\bar{2}2$ ) semi-polar GaN has been obtained by overgrowth on nanorod templates, which were fabricated using our self-organized nickel nano-mask technique.<sup>6,7</sup> Four samples, each with five periods of InGaN/GaN MQWs were grown on the overgrown (11 $\bar{2}2$ ) GaN. The four samples have similar structures, but with different indium content. In each case, the quantum well and the barrier are 3 nm and 10 nm thick, respectively. For simplicity, the four samples are labelled as samples A, B, C, and D, corresponding to indium compositions of approximately 13%, 24%, 29%, and 35%, respectively. TRPL measurements have been performed using a time-correlated single photon counting (TCSPC) system using a 375 nm pulsed diode laser with a pulse width of 83 ps

<sup>a)</sup> Author to whom correspondence should be addressed. Electronic mail: [t.wang@sheffield.ac.uk](mailto:t.wang@sheffield.ac.uk)

as an excitation source. The luminescence was dispersed using a 0.55 m monochromator and detected by a thermoelectrically (TE) cooled charge coupled device detector (CCD). The samples were mounted into a closed-circuit helium cryostat to implement temperature-dependent TRPL from 7 to 300 K. Spatially resolved PL measurements have been conducted at room temperature by means of a commercial confocal PL system with a spatial resolution of  $\sim 160$  nm. The scanning areas range from  $3 \times 3$  to  $10 \times 10 \mu\text{m}^2$  with a step size varied between 20 and 100 nm.

Figure 1(a) gives the time-integrated PL (TIPL) spectra of all samples measured under identical conditions at 7 K, showing that the peak emission wavelength increases from 425 to 505 nm with increasing the indium content. It is worth highlighting that the PL intensity does not drop significantly with increasing indium content even up to 35%, corresponding to emission in the green spectral region, demonstrating the major advantage of semipolar InGaN/GaN MQWs compared to polar c-plane counterparts. The linewidths of the emission peaks also increase with increasing indium content, implying enhanced indium segregation. Furthermore, all the emission peaks show an asymmetric shape, which has been observed even for the MQWs with a low indium content.<sup>15</sup>

Figure 1(b) shows the TRPL traces of all samples measured under identical conditions at 7 K. In addition, the measured system response trace is included. For comparison, Figure 1 also includes the data from a polar blue InGaN/GaN MQWs sample grown on c-plane sapphire. Compared with the TRPL trace of the polar blue InGaN/GaN MQWs, the TRPL traces of all the semi-polar samples show a considerably faster initial decay. This has also been observed on InGaN/GaN MQWs grown on free-standing GaN substrates.<sup>9–13</sup> A standard two exponential component model is used to study excitonic dynamics, and thus TRPL traces  $I(t)$  can be described by<sup>16–18</sup>

$$I(t) = A_1 \exp(-t/\tau_1) + A_2 \exp(-t/\tau_2). \quad (1)$$

$A_1$  and  $\tau_1$  ( $A_2$  and  $\tau_2$ ) are the fast (slow) decay components. The fitting results are plotted in dashed lines shown in Figure 1(b), as we have previously demonstrated on different

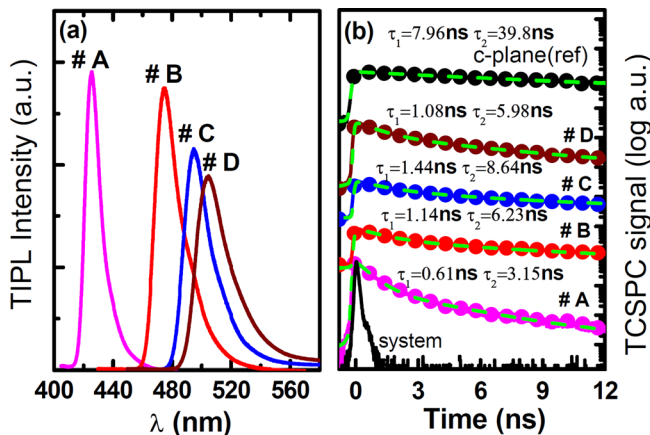


FIG. 1. (a) TIPL spectra and (b) TRPL trace of all samples, measured under identical conditions at 7 K.

structures.<sup>16</sup> For all the semipolar samples, i.e., samples A–C, the lifetime of the fast decay component at 7 K gradually increases from 0.61 ns (sample A) through 1.14 ns (sample B) to 1.44 ns (sample C). This implies that the radiative recombination lifetime increases with increasing indium composition from 13% to 29%. This is due to the increased QCSE as a result of the enhanced strain, which leads to the enhanced separation of the electron and hole wavefunctions. These lifetime values are significantly shorter than those of the polar c-plane blue MQW which is about 7.96 ns. Furthermore, our previous study shows that the radiative lifetime of a c-plane green MQW sample with a similar structure was reported to be as long as 57.2 ns.<sup>16</sup> Therefore, it can be concluded that the polarization effect in semi-polar MQWs is significantly reduced.

The most remarkable point is for sample D with an indium content of 35%, where the QCSE becomes even stronger as a further increased lattice mismatch between  $\text{In}_{0.35}\text{Ga}_{0.65}\text{N}$  and GaN. However, Figure 1(b) shows that the lifetime of the fast decay component decreases to 1.08 ns. Based on the well-established knowledge of c-plane InGaN/GaN MQWs, potential fluctuations and localization centres can play a significant role in the recombination processes of InGaN quantum wells.<sup>19</sup> Further studies of exciton localization have been carried out by investigating temperature/excitation power-dependent TRPL and high spatial-resolution confocal PL measurements.

Figures 2(a) and 2(b) show the excitation-power dependent TIPL spectra and the excitation-power dependent traces of the TRPL, respectively, both measured at room temperature. Figures 2(c) and 2(d) provide both the wavelength of the emission peak and the lifetime of the fast decay component as a function of photo-generated carrier density (i.e., excitation power), extracted from Figures 2(a) and 2(b), respectively. The photo-generated carrier density  $N_{\text{photon}}$  can be estimated by the following equation:<sup>20</sup>

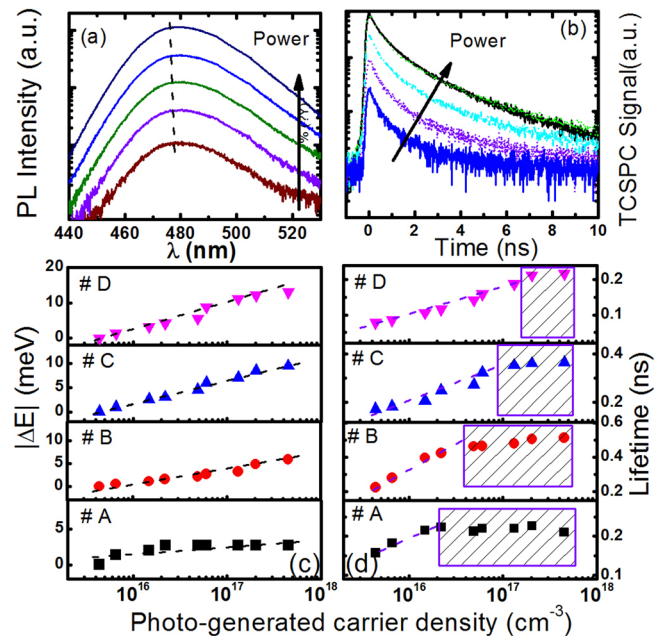


FIG. 2. Excitation-power dependent (a) TIPL spectra and (b) TRPL traces of sample B as an example, respectively. (c) Emission peak wavelength and (d) PL lifetime as a function of photo-generated carrier density for all samples. All are measured at room temperature.

$$N_{\text{photon}} = \frac{P}{(h\nu) \times \phi \times d_{\text{active}} \times f} \times [1 - \exp(-\alpha_{\text{InGaN}} d_{\text{InGaN}})] \times (1 - R), \quad (2)$$

where  $P$  is the power of pumping laser;  $h\nu$  is the energy of injected photon;  $\phi$  is the spot size of laser beam;  $d_{\text{InGaN}}$  and  $\alpha_{\text{InGaN}}$  are the thickness and absorption efficiency of InGaN active layer, respectively;  $f$  is the repetition rate of laser used; and  $R$  is the reflectance, which can be estimated by using refractive indices of air and GaN. A 375 nm pulsed laser with a repetition rate of 20 MHz was used, and the laser beam was focused down to a spot of  $\sim 25 \mu\text{m}$  diameter. The excitation power density used ranges from 0.69 to 71 kW/cm<sup>2</sup>. For our measurements, we have  $\phi = 25 \mu\text{m}$ ,  $d_{\text{InGaN}} = 15 \text{ nm}$ ,  $\alpha_{\text{InGaN}} = 10^5 \text{ cm}^{-1}$ , and  $R = 0.17$ . Consequently,  $N_{\text{photon}}$  has been estimated to range from  $4.4 \times 10^{15}$  to  $4.5 \times 10^{17} \text{ cm}^{-3}$ . Figure 2(c) shows that the blue shift in emission energy  $|\Delta E|$  increases from 3 to 13 meV as the indium composition increases from 13% to 35%. The evolution of the lifetime of the fast decay component is shown with increasing photo-generated carrier density in Figure 2(d). Under low photo-generated carrier density, the lifetime of the fast decay component is short, as non-radiative recombination dominates the carrier recombination process. An increase in lifetime of the fast decay component is observed for increasing photo-generated carrier density. It is expected that this is related to the saturation of some nonradiative recombination channels. The increase in the lifetime of the fast decay component with increasing carrier density saturates for sample A when the photo-generated carrier density is above  $2 \times 10^{16} \text{ cm}^{-3}$ . The saturation point is gradually shifted to higher power densities with increasing indium content, as marked by the shadowed areas in Figure 2(d).

Temperature dependent TRPL measurements have been performed. As an example, Figure 3(a) shows the

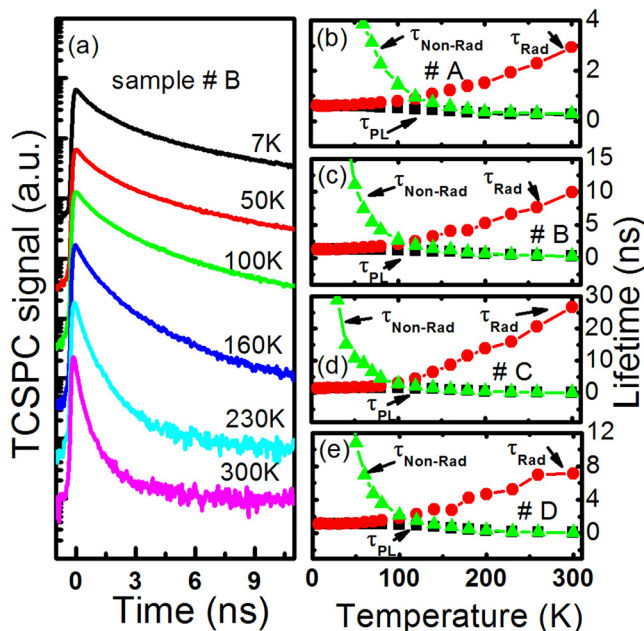


FIG. 3. (a) Temperature dependent TRPL traces measured from 7 to 300 K using sample B as an example. (b)–(e):  $\tau_{\text{PL}}$ ,  $\tau_{\text{R}}$ , and  $\tau_{\text{NR}}$  of samples A, B, C, and D as a function of temperature from 7 to 300 K.

temperature dependent TRPL trace of sample B. Radiative recombination lifetime ( $\tau_{\text{R}}$ ) and non-radiative recombination lifetime ( $\tau_{\text{NR}}$ ) are obtained based on an approach proposed by Marcinkevicius *et al.*<sup>22,23</sup>

$$\tau_{\text{R}} = \tau_{\text{PL}} \times (I_{t-p}(T)/I_{t-p}(7\text{K}))^{-1} \quad \text{and} \quad 1/\tau_{\text{PL}} = 1/\tau_{\text{R}} + 1/\tau_{\text{NR}}, \quad (3)$$

where  $I_{t-p}(T)$  is the PL transient peak after the excitation at the corresponding temperature.

Figure 3(b) shows the radiative recombination lifetime ( $\tau_{\text{R}}$ ) and non-radiative recombination lifetime ( $\tau_{\text{NR}}$ ) of all samples as a function of temperature from 7 to 300 K. For sample A with an indium composition of 13%,  $\tau_{\text{R}}$  at 7 K and 300 K is 0.63 ns and 2.93 ns, respectively, both of which are much faster than that of c-plane MQWs. The corresponding  $\tau_{\text{NR}}$  at 7 K and 300 K is 23.8 ns and 0.29 ns, respectively. The transition temperature,<sup>12</sup> where the dominating emission mechanism changes from radiative to non-radiative recombination, is 160 K. When the indium content increases to 24%, i.e., sample B, the transition is reduced to 120 K as a result of the increased polarization effect.<sup>16</sup> Furthermore, the  $\tau_{\text{R}}$  of sample B is 9.9 ns at RT, which is longer than that of sample A. For sample C, the transition further reduces to 100 K, and the  $\tau_{\text{R}}$  further extends to 26.6 ns.

The most interesting behaviour is found in sample D, where the polarization effect is further enhanced as a result of increased indium content. However, Figure 3(e) shows that the increasing trend of the  $\tau_{\text{R}}$  is greatly suppressed when the temperature is above 120 K. The  $\tau_{\text{R}}$  even remains as fast as 7.14 ns at RT. Therefore, this means that the optical emission mechanism for semi-polar InGaN/GaN MQWs with high indium content is dominated by exciton localisation effects rather than the QCSE, which is significantly different from high indium content MQWs on the polar c-plane. This also implies that growth of InGaN/GaN MQWs along the semi-polar (11 $\bar{2}$ 2) orientation offers the potential of achieving high efficiency green or even yellow emission.

The exciton localization as a result of indium segregation has been confirmed by detailed confocal PL measurements. The PL mapping measurements have been performed at room temperature on all samples with a scanning area of  $3 \times 3 \mu\text{m}^2$  and a step size of 20 nm. In order to make a clear comparison, Figures 4 and 5 show mapping of the peak wavelength and the full width at half maximum (FWHM) of the peak emission from samples A and D, respectively. The peak wavelength of the emission from sample A fluctuates from 429 to 434 nm and the FWHM from 19 to 25 nm as shown in the histograms given in Figure 4(c), while the range of the data for sample D shown in Figure 5 is much larger as a result of the significantly higher indium content in sample D. Table I summarizes all parameters obtained from the confocal PL mapping measurements on samples A–D, indicating that with increasing indium content, the ranges in both the peak wavelength and the FWHM of the emission peaks progressively increase from 0.7 to 3.0 nm and from 1.1 to 3.1 nm, respectively. These features indicate enhanced exciton localization as a result of increasing indium content. Furthermore, it has been found that a clear spatial correlation exists between the emission peak wavelength and the

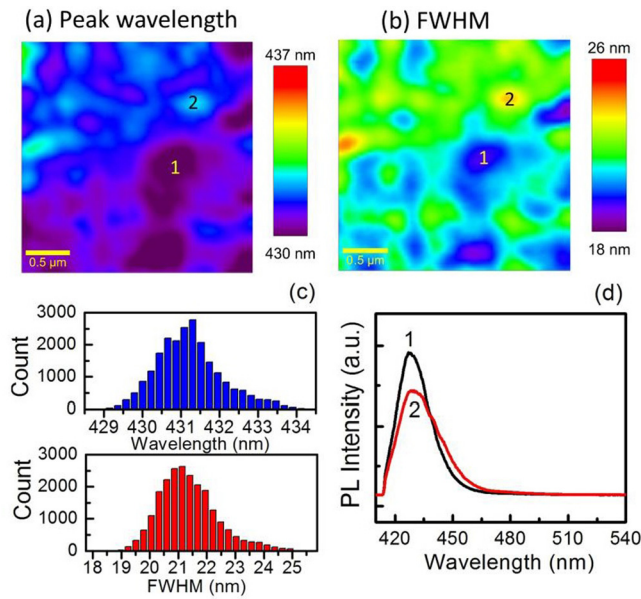


FIG. 4. Mapping of the emission peak wavelength (a); FWHM of the emission peak of sample A (b); Deviations of the peak wavelength and the FWHM (c); and PL spectra taken from the areas labelled as “1” and “2” in sample A (d).

FWHM of the emission peak. For example, for sample A, the spectra taken from the areas labelled as “1” and “2” are shown in Figure 4(d), while Figure 5(d) shows the spectra taken from the areas labelled as “3” and “4” of sample D. The differences between the points in Figures 4(d) and 5(d) in PL intensity and peak wavelength are significantly increased for sample D. Furthermore, multiple PL peaks have been observed as shown in Figure 5(d). These results confirm the formation of local potential fluctuations leading to exciton localization in semi-polar MQWs as a result of increasing indium content.

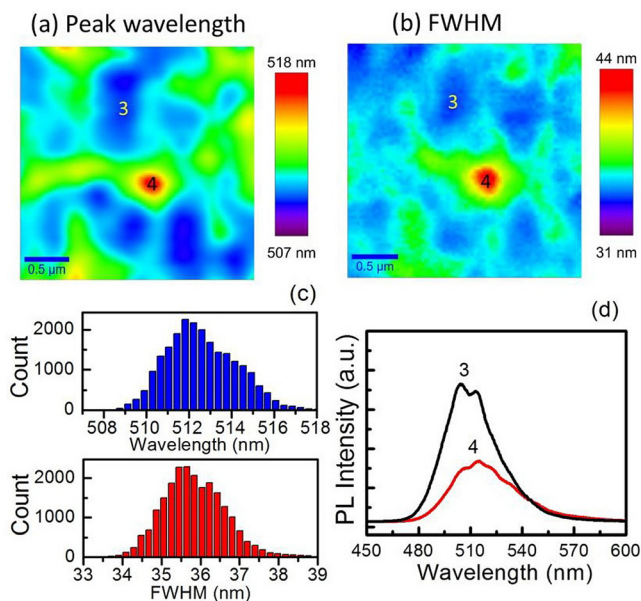


FIG. 5. Mappings of the emission peak wavelength (a) and the FWHM of the emission peak of sample D (b); Deviations of the peak wavelength and the FWHM (c); and PL spectra taken from the areas labelled as “3” and “4” in sample D (d).

TABLE I. Parameters obtained from confocal PL measurements.

Sample number	A	B	C	D
In composition $x$ (%)	13	24	29	35
Average peak wavelength (nm)	431.3	487.2	506.3	514.7
Peak wavelength deviation (nm)	0.7	1.9	2.5	3.0
Average FWHM (nm)	21.5	28.2	32.8	36
FWHM deviation (nm)	1.1	1.9	2.8	3.1

In summary, a temporally and spatially resolved optical investigation has been carried out on  $\text{In}_x\text{Ga}_{1-x}\text{N}/\text{GaN}$  ( $13\% \leq x \leq 35\%$ ) MQWs grown on the (11 $\bar{2}$ 2) semi-polar GaN with high crystal quality, achieved through overgrowth on nanorod templates. The radiative recombination lifetime increases with increasing indium content as expected before reaching the green emission region. Further increasing the indium content to generate green emission leads to a faster radiative recombination lifetime, which is different from  $\text{InGaN}/\text{GaN}$  MQWs grown on polar  $c$ -plane sapphire where the QCSE plays the dominant role in the emission process. The reduced radiative recombination lifetime is due to the formation of sub-micron localization centres in local potential fluctuations as a result of the high indium content, while the QCSE does not play an important role due to the semipolar orientation of the  $\text{InGaN}/\text{GaN}$  MQWs. The formation of the exciton localization centres has been confirmed by our detailed confocal PL measurements.

This work was supported by the UK Engineering and Physical Sciences Research Council (EPSRC).

- <sup>1</sup>P. Waltereit, O. Brandt, A. Trampert, H. T. Grahn, J. Menniger, M. Ramsteiner, M. Reiche, and K. H. Ploog, *Nature* **406**, 865 (2000).
- <sup>2</sup>T. Takeuchi, H. Amano, and I. Akasaki, *Jpn. J. Appl. Phys., Part 1* **39**, 413 (2000).
- <sup>3</sup>Y. Zhao, S. H. Oh, F. Wu, Y. Kawaguchi, S. Tanaka, K. Fujito, J. S. Speck, S. P. DenBaars, and S. Nakamura, *Appl. Phys. Express* **6**, 062102 (2013).
- <sup>4</sup>D. S. Kim, S. Lee, D. Y. Kim, S. K. Sharma, S. Hwang, and Y. G. Seo, *Appl. Phys. Lett.* **103**, 021111 (2013).
- <sup>5</sup>P. S. Hsu, F. Wu, E. C. Young, A. E. Romanov, K. Fujito, S. P. DenBaars, J. S. Speck, and S. Nakamura, *Appl. Phys. Lett.* **103**, 161117 (2013).
- <sup>6</sup>K. Xing, Y. Gong, J. Bai, and T. Wang, *Appl. Phys. Lett.* **99**, 181907 (2011).
- <sup>7</sup>J. Bai, Y. Gong, K. Xing, X. Yu, and T. Wang, *Appl. Phys. Lett.* **102**, 101906 (2013).
- <sup>8</sup>J. E. Northrup, *Appl. Phys. Lett.* **95**, 133107 (2009).
- <sup>9</sup>M. Funato, A. Kaneta, Y. Kawakami, Y. Enya, K. Nishizuka, M. Ueno, and T. Nakamura, *Appl. Phys. Express* **3**, 021002 (2010).
- <sup>10</sup>G. A. Garrett, H. Shen, M. Wraback, A. Tyagi, M. C. Schmidt, J. S. Speck, S. P. DenBaars, and S. Nakamura, *Phys. Status Solidi C* **6**(S2), S800 (2009).
- <sup>11</sup>A. Kaneta, Y. S. Kim, M. Funato, Y. Kawakami, Y. Enya, T. Kyono, M. Ueno, and T. Nakamura, *Appl. Phys. Express* **5**, 102104 (2012).
- <sup>12</sup>S. Marcinkevičius, Y. Zhao, K. M. Kelchner, S. Nakamura, S. P. DenBaars, and J. S. Speck, *Appl. Phys. Lett.* **103**, 131116 (2013).
- <sup>13</sup>S. Marcinkevičius, R. Ivanov, Y. Zhao, S. Nakamura, S. P. DenBaars, and J. S. Speck, *Appl. Phys. Lett.* **104**, 111113 (2014).
- <sup>14</sup>S. Marcinkevičius, K. Gelžinytė, Y. Zhao, S. Nakamura, S. P. DenBaars, and J. S. Speck, *Appl. Phys. Lett.* **105**, 111108 (2014).
- <sup>15</sup>L. Schade, U. T. Schwarz, T. Wernicke, J. Rass, S. Ploch, M. Weyers, and M. Kneissl, *Appl. Phys. Lett.* **99**, 051103 (2011).
- <sup>16</sup>B. Liu, R. Smith, J. Bai, Y. Gong, and T. Wang, *Appl. Phys. Lett.* **103**, 101108 (2013).
- <sup>17</sup>S. F. Chichibu, K. Hazu, Y. Ishikawa, M. Tashiro, H. Namita, S. Nagao, K. Fujito, and A. Uedono, *J. Appl. Phys.* **111**, 103518 (2012).

- <sup>18</sup>J. H. Na, R. A. Taylor, K. H. Lee, A. M. Fox, T. Wang, P. Parbrook, S. N. Yi, J. W. Choi, and J. S. Lee, *Appl. Phys. Lett.* **89**, 253120 (2006).
- <sup>19</sup>Y. Kawakami, Y. Narukawa, K. Sawada, S. Saijyo, S. Fujita, S. Fujita, and S. Nakamura, *Mater. Sci. Eng. B* **50**, 256 (1997).
- <sup>20</sup>Y. J. Lee, C. H. Chiu, C. C. Ke, P. C. Lin, T. C. Lu, H. C. Kuo, and S. C. Wang, *IEEE J. Sel. Top. Quantum Electron.* **15**, 1137 (2009).
- <sup>21</sup>M. Funato and Y. Kawakami, *J. Appl. Phys.* **103**, 093501 (2008).
- <sup>22</sup>S. Marcinkevičius, K. M. Kelchner, L. Y. Kuritzky, S. Nakamura, S. P. DenBaars, and J. S. Speck, *Appl. Phys. Lett.* **103**, 111107 (2013).
- <sup>23</sup>E. Berkowicz, D. Gershoni, G. Bahir, E. Lakin, D. Shilo, E. Zolotoyabko, A. C. Abare, S. P. DenBaars, and L. A. Coldren, *Phys. Rev. B* **61**, 10994 (2000).